Evidence of quantum consciousness in evoked zero-spin echoes

Christian Kerskens and David López Pérez
Institute of Neuroscience, Trinity College, Dublin, Ireland

That consciousness could have its' basis in quantum computing has been speculated for many years [1]. Unfortunately, unitary quantum gates, the main ingredient of quantum computing [2], are not compatible with irreversible biological systems which are effectively non-unitary. That is why Penrose and Hameroff [3, 4] have suggested and Hagan et al. have theoretically confirmed [5] that long lasting coherent states may exist in microtubuli of the neuron's cytoskeleton. Furthermore, it has been argued that microtubular processes are linked to consciousness because of how they are affected by anaesthetics [6]. However, no experimental evidence exists so far that could connect consciousness to quantum computing. Here, we used magnetic resonance imaging (MRI) to study long-range quantum coherence in the human brain. We were surprised to find that the cardiac pressure pulse evoked zero-spin echoes (ZSEs) in brain parenchyma. The ZSE signals, which are thought to be generated by long-range intermolecular zero-quantum coherence (iZQC) [7], were much higher than expected. In contrast, single quantum coherence (SQC) imaging, which is also indirectly related to iZQC, was not affected. These findings suggest that we observed a non-classical effect originated from a small subdomain of the parenchyma. This evoked quantum effect was directly connected to consciousness as only sporadic ZSE signals were detected during sleep while a loss of the evoked quantum effect would probably always result in unconsciousness. We concluded, that the observed quantum phenomenon must be a necessity for consciousness. Our findings are unexpected but in line with recent biological research [8–12] and further theoretical results [13, 14], which have been shown that quantum coherence and entanglement can play an important role in biology.

INTRODUCTION

MRI provides a non-invasive way to detect long-range intermolecular multiple-quantum coherence (iMQC) via dedicated multiple spin echo (MSE) sequences [15–17]. In the quantum mechanical formalism by Warren [18, 19], where all dipolar-couplings are taken into account explicitly, only those contributions dominate which also retain the classical formalism [20] that was initially introduced to describe MSE [15–17]. The classical formalism is retained because it is assumed that the dynamics are a collective effect of a classical fluid. Despite the dipole field angulation, MSEs have always a similar signal contrast in single-quantum coherence (SQC), mainly because short-range iMQC also influences SQC via T_1 and T_2 relaxation and while long-range iMQC do so via proton nuclear magnetic resonance line narrowing. For MSE sequences, asymmetric magnetic field gradients (asymmetric integrated over time) are applied in combination with at least two radio-frequency (RF) pulses [15–17]. This situation is present in fast repeated single-slice gradient-echo echo planar imaging (GE-EPI) series, where so-called crusher gradients (to dephase any SQC signal that remains from the previous excitation) are added between two acquisitions (see figure 7). This scheme could result in a ZSE component in every second image but the ratio of the associated iZQC to SQC of the gradient-echo only reaches up to 0.02 at 4 T experimentally [7, 21]. At 3 T and without an optimized sequence, this ratio should be substantively lower, which means that the iZQC signal is negligible in fast imaging series due to low signal-to-noise. In our experiments, we used a conventional GE-EPI series with a short repetition time (TR) and two additional saturation pulses. The saturation pulses were introduced to increase long-range correlation via the additional gradients of the saturation pulses by a factor of around 6.

RESULTS

With this sequence, we found predominant alternations with the cardiac frequency in brain tissue. In each cardiac cycle, we observed a period which varied in length between 150 and 420 ms showing an alternating signal of up to 15 % as plotted in Figure 1 and 2A to which we will refer to in the following as zigzags.

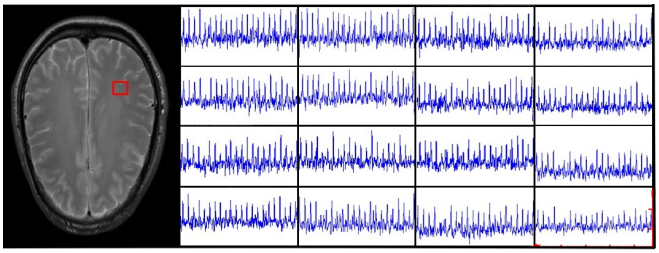

Figure 1. A 4x4 voxel matrix randomly picked. On the left, the red square shows location in the brain slice. On the right, 16 corresponding signal time courses of 24 s displaying the local tissue responses.

The zigzags as shown in Figure 2A were achieved using additional cushions inside the coil and by breath-holding (without taking a deep breath). Breath-holding showed an immediate increase in zigzags (up to 4-5 peaks) but no

delayed response to the PCO_2 challenge as we found in the blood vessels (not shown here). Under normal condition, the zigzags usually only contain two or three peaks as shown in Figure 2B (during the first 10 s from 50 s to 60 s). At 60 s, the volunteer was instructed to hyperventilate with the result that the zigzags immediately disappeared.

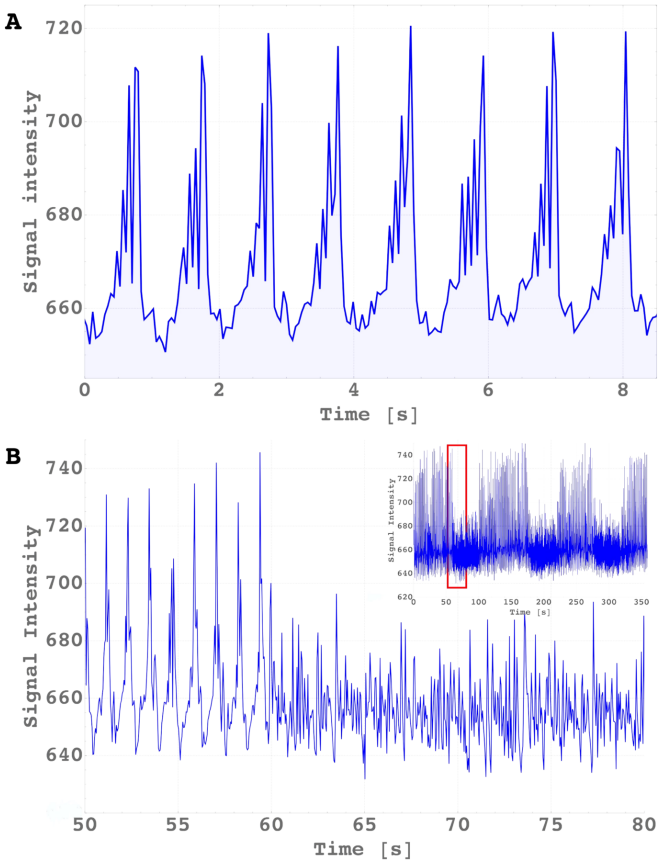

Figure 2. **A**: Whole-slice averaged signal time course (selected by a mask) during 8 heart cycles. Subject had extra head fixation and was instructed to breath-hold during the period. In contrast to signals in the veins (not shown here), zigzag signal showed no response to CO2 activity other than an immediate lengthening of the zigzag. **B**: Whole-slice averaged signal time course during normal breathing first. At 60 s, the subject was instructed to hyperventilate. The inlet shows the total time course with 3 hyperventilation periods and the selected time interval in red.

We found zigzags in all participants who were instructed to stay awake. Prior to this instruction, we found a signal decline in participants which had fallen asleep as illustrated in Figure 3.

We used an finger pulse oximeter and MRI data of the superior sagittal sinus to find reference time frames for the zigzag pattern. We found that the zigzags always appeared during the arterial inflow phase. The abrupt end of the zigzags were coincident with the end-phase of

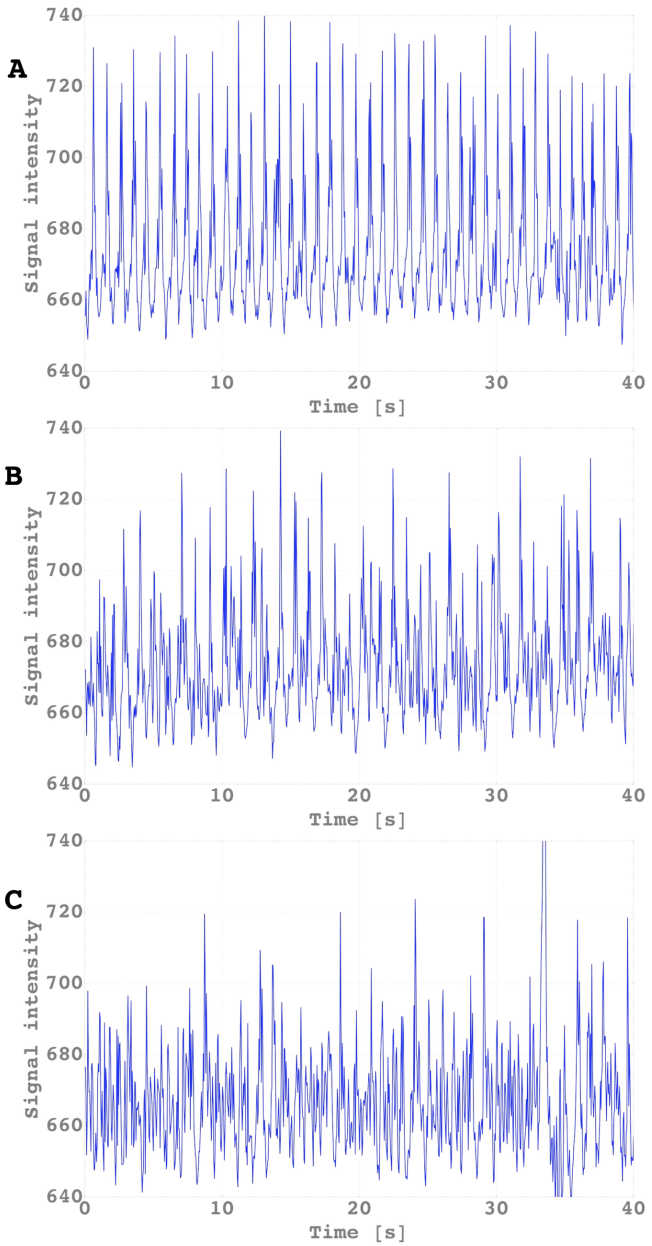

Figure 3. Pattern observed in participant who had reported falling asleep. We recognized two phases. B: First phase showed a fluctuation of the maximum peak intensity and an increase of random signals between maximum peaks. C: In the second phase, the maximum peaks decline with a further increase of the noise level between peaks. At 34 s, the peak resulted from short head movement.

the arterial pulse as shown in Figure 4A and the rise of venous outflow as demonstrated in Figure 4B.

We located the zigzags over the entire brain tissue except in the periventricular area as shown in Figure 5, regions like skull, ventricle etc and in the attached test

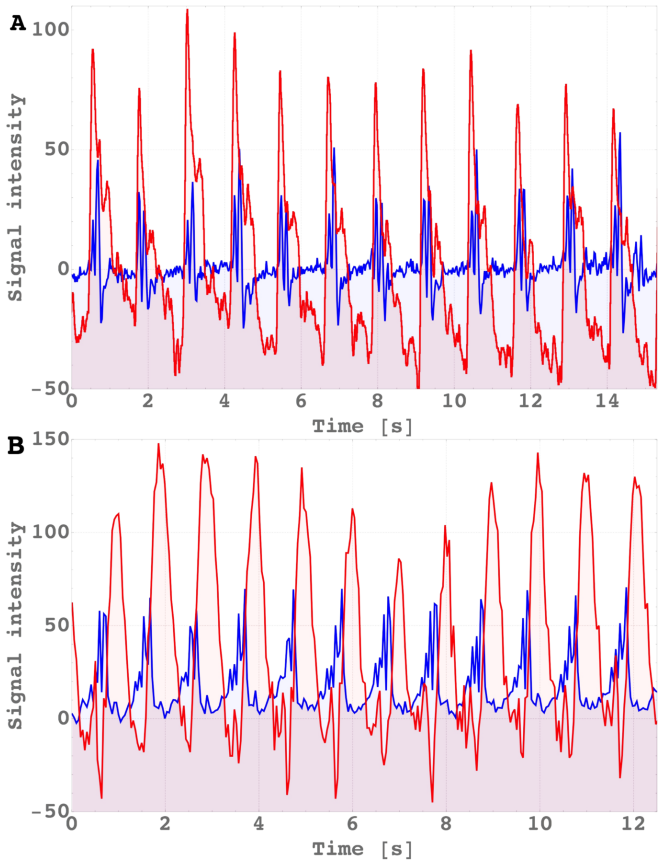

Figure 4. Signal time course (Blue) during 12 heart cycles compared with **A**: Simultaneous oximeter reading of a finger (Red) and **B**: Signal time course (Red) of a vein.

tubes. The zigzag, including the sudden end, could be restored while being averaged over the whole imaging slice Figure 2A.

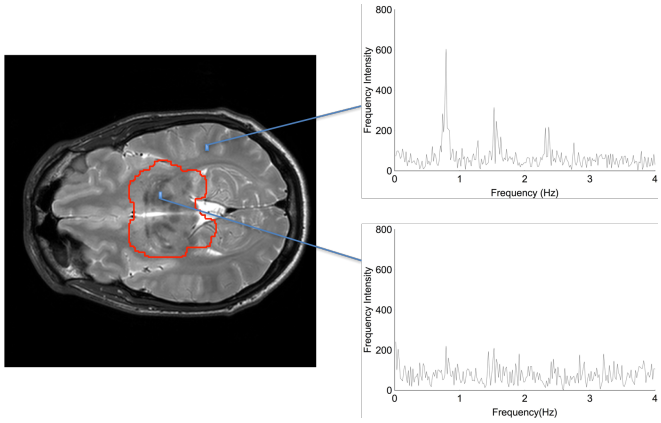

Figure 5. Fourier-Transform of two representative voxel. Surrounded tissue (red drawing) on the left shows signal dependency as shown in the bottom plot.

For varying the slice angulation, we found an angle dependency of the demagnetization field as shown in Figure 6A where φ is the angle between the slice gradient and the main magnet field. The plot represents the fitted function $|(3 \cdot cos^2[\varphi_{cor}] - 1)|$ where φ_{cor} takes additional gradients in read direction into account. Adjusted R^2 test of goodness-of-fit resulted in R^2=0.9958.

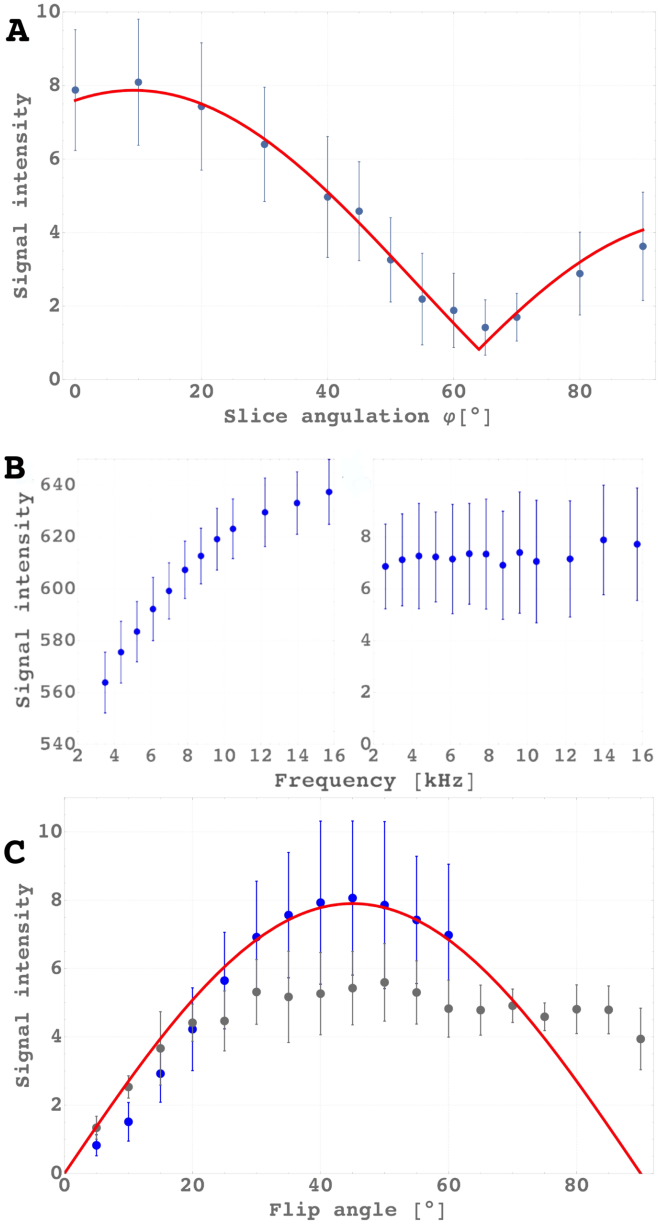

Figure 6. Variation of sequence parameters. Data shows signal averaged over 5 subjects. Error bars represent the standard deviation from the mean. **A**: Signal intensity plotted against the slice gradient angulation φ in respect to the magnetic main field. **B**: Signal intensity plotted against the frequency offset of the saturation slices of the averaged baseline signal (left) and averaged signal of cardiac pattern (right). **C**: Whole-slice averaged signal time course plotted against flip angle variation with saturation pulses (Blue) and without (Grey). IZQC prediction plotted in Red.

For off-resonance frequency variation, we found a typical magnetization transfer contrast (MTC) change for the baseline signal which depended on the off-resonance frequency (Figure 6B, left-hand side). In contrast, the zigzag intensity showed no significant changes in the same frequency range (Figure 6B, right-hand side).
For flip angle variation, we found a maximum peak intensity at 45° (Figure 6C). The predicted signal course for iZQC [22] was fitted to the data (R^2=0.9964).
Without saturation, we could extend our observation to 90° where we found a flat plateau following an initial signal increase. In comparison, with (c) the signal was lower from 25° onward as shown in Figure 6C. This was due to slice angulation which resulted in a gradient angulation of $\varphi_{cor} = 9.6°$ and $\varphi_{cor} = 45°$, respectively, meaning that without saturation the signal was reduced by nearly half due to the angulation.

DISCUSSION

We found an alternating signal component (zigzags) meeting expectation of iZQC which included firstly, that it only appears after an RF-pulse—gradient—RF-pulse scheme (therefore alternating); secondly, that the signal manifests a characteristic angulation dependency of its dipole-dipole interaction (Figure 6A); thirdly, that it showed, when the saturation pulses were applied, the remarkable immunity to MTC [23] (Figure 6B) and fourthly, that the flip angle is optimal at 45° [22] (Figure 6C). Figure 6C shows also data without the saturation pulses. There, the correlation length was very short due to the missing gradients from the saturation which resulted in destructive coherences (signal plateau from 30° onward) [24] . It shows that our sequence was optimised for iZQC but in general the physiological mechanism behind our observation evoked multiple quantum coherences.
We could confirm that the iZQC signal is prone to movement from the following observations. In hyperventilation challenges, the signal declined immediately at the start of the challenge before any cerebral blood flow response. Further, in same areas which were subject to movement like the the periventricular area [25], we found no trace of iZQC. Otherwise, we found that reduced body movement through breath-holding, resulted in an immediate lengthening of the signal response. Surprisingly, the signal in the breath-holding experiment did not respond to the CO_2 challenge, despite the fact, that we observed increased blood flow in major blood vessels (data not shown here). Furthermore, we found in a fMRI study [26], that local increase in blood perfusion during visual activation left the zigzag undisturbed. We concluded that the signal was evoked by the pressure wave and not by arterial blood flow. The iZQC signal was not accompanied by any other MRI contrast changes. The missing SQC component ruled out that the signal was generated by changes in T_1 and T_2 relaxation, line narrowing, or magnetic field. The direct relation of iMQC to T_1 and T_2 relaxation or the line narrowing, excluded the possibility of a collective effect of the bulk water including effects like a broken spherical symmetries through restricted diffusion or similar, the main contrast mechanism in iMQC. This has also been confirmed in diffusion-studies of the cardiac cycle [25]. From the missing field shift, we can reject our initial presumption that a broken mirror symmetry [27] may produce iMQC. We realized that it can be shown with the help of perturbation theory that a broken mirror symmetry would produce a field shift [28]. Further, the fact that the signal was by a magnitude higher than expected led us to believe that the classical formalism of MSE is not sufficient. We concluded that in Warren's formalism other contributions than in a classical liquid may dominate the coherence pathway. Consequently, brain tissue cannot be treated as a classical liquid. From the mismatch between the high signal change in ZSE and no significant change in SQC, we follow that the compartment producing the ZSE signal is small or invisible to SQC through short relaxation times. In either cases, the quantum phenomenon could be also an entanglement as shown in solid state [29]. What does this mean for the brain? We had realized that the signal can decline during sleep. The decline happened gradually, whereby the peaks remained at first (which means that movement didnot cause the change) but the noise level between increased. Then, it followed a phase were peaks also declined, resulting in a noisy signal with sporadic peaks. Therefore, we asked the participants of the final part of the study to stay awake. As a result, we found no delining signals in any of the participants. From this, we conclude that the signal was always present during consciousness. Further we found that the signal showed a perfect synchronization with the cardiac pulse but was not flow-related. Therefore, we can assume that during a vasovagal syncope [30], where cardiac pulsation is disturbed through a sudden pressure drop, no quantum phenomenon can be evoked. Consequently, the immediate unconsciousness could be the result of the missing quantum phenomenon. For the reason that pressure pulse variation do not correlate with sleep directly but the quantum phenomenon did we believe that missing the quantum phenomenon is the initial cause of unconsciousness. We conclude that the evoked quantum phenomenon is a necessity for consciousness.

METHODS

40 subjects (between 18 and 46 years old) were scanned in a 3.0 T Philips whole-body MRI scanner (Philips, The Netherlands) operated with a 32-channel array receiver coil. Imaging protocols using standard single-shot GE EPI sequence were approved by the Trinity College School of Medicine Research Ethics Committee. In our consecutive EPI time series, only even-numbered readouts contained MSEs (whereby counting begins one read-

out before the broken symmetry occurs). The asymmetric gradient field (Figure 7), which are before the even-numbered slice-selection RF-pulses, generated then zero quantum orders [31] and higher negative orders []. Initial experiments were carried out to establish a protocol that could deliver stable cardiac related signals over a range of subjects. Initially, test tubes with a water solution (1000 ml demineralized water contained 770 mg $CuSO_45H_2O$, 1 ml Arquad (AkzoNobel), 0.15 ml H_2SO_4-(0.1 N)) were positioned close to the head for reference signals. The finalized parameters of the GE-EPI sequence were as follows: FA = 45°, TR = 45 ms and the TE = 5 ms with a voxel size was 3.5 x 3.5 x 3.5 mm, matrix size was 64x64, SENSE factor 3, bandwidth readout direction was 2148 Hz.

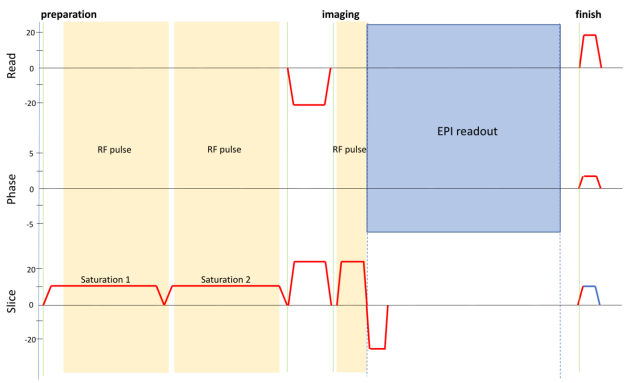

Figure 7. Gradient scheme of the EPI sequence with two saturation pulse.

Figure 7 shows the gradient scheme. Saturation gradients had a time integral (length x strength) of $\mathrm{Gt}_{sat} = 5.1$ ms x 6.25 mT/m, the crusher gradients in read and slice direction of $\mathrm{Gt}_{cru} = 1.3$ ms x 25 mT/m, the slice rephase gradient of $\mathrm{Gt}_{sr} = 0.65$ ms x 25 mT/m, the slice termination gradient of $\mathrm{Gt}_{st} = 0.65$ ms x 15 mT/m, and the total read dephase after EPI readout gradient of $\mathrm{Gt}_{rt} = 0.65$ ms x 22.5 mT/m. The angle between magnet field and gradient field was then

$$\varphi_{cor} = \varphi - \tan^{-1}\left[\frac{\mathrm{Gt}_{cru} - \mathrm{Gt}_{rt}}{2\mathrm{Gt}_{sat} + \mathrm{Gt}_{cru} + \mathrm{Gt}_{st}}\right] = \varphi - 9.6^\circ$$

where φ is the slice angulation. The imaging slice was set coronal above the ventricle. In addition, two saturation slices of 5 mm (15mm above and 20mm below) in thickness were placed parallel to the imaged slice. During our initial experiments, we realized that participants who had fallen asleep didn't show the desired signal pattern. From 7 initial data sets with no zigzag pattern, two had reported to have fallen asleep. Therefore, all participants of final data acquisition were asked to stay awake during the imaging protocol which eliminated the problem. The following alternation (each with 1000 repetitions in five participants) were carried out, (a) slice angulation starting from coronal 0° to axial 90°in the steps as [0, 10, 20, 30, 40, 45, 50, 55, 60, 65, 70, 80, 90], (b) the distance of the REST slabs were varied between 0.8 mm and 50 mm to alter the off-resonance frequency. The off-resonance frequencies were [2.62, 3.49, 4.36, 5.23, 6.11, 6.98, 7.84, 8.73, 9.60, 10.47, 12.22, 13.96, 15.71, 17.45] kHz, (c) Flip angle was varied for the case with saturation pulses from 5° to 60° in steps of 5°(60°was the power limit by the specific absorption rate (SAR)) and without saturation pulses from 5°to 90° in steps of 5°, (d) 9 slices were acquired at different positions, with each slice matching from bottom to the top the position of those acquired in the anatomical scan. In four participants, we examined the motion sensitivity where we immobilized the head with multiple cushions. During indicated intervals the subjects were asked to stop breathing for 20 s or to hyperventilate for 40 s. Finally, anatomical MRI images in all studies included a high-resolution sagittal, T1-weighted MP-RAGE (TR = 2.1 s, TE = 3.93 ms, flip angle = 7).

Data were processed with Matlab 2014a (http://www.mathworks.co.uk/). Rescaling was applied to all data sets before any analysis using the MR vendor's instructions. Average time series were visually inspected in search for irregularities which were manually removed from the analysis leaving the rest of the time series unaltered. Manual segmentation was used to create a mask to remove cerebral spinal fluid (CSF) contributions. The first 100 scans were removed to avoid signal saturation effects. The manual segmentation of the masks was eroded to avoid partial volume effects at the edges. The cardiac signal and baseline detection was based on the method proposed in Gomes and Pereira [32]. Final data presentation was carried with Mathematica (Wolfram Research, Champaign, Illinois).

Authors' contributions

Software, validation, formal analysis, investigation, data curation by D.L.P.; Conceptualization, methodology, writing (original draft), supervision, funding acquisition by C.K.

Acknowledgments

We would like to thank S. Joseph for carrying out the imaging protocols for our participants, R. Fallon for reading the manuscript, and Science Foundation Ireland for supporting D.L.P. from 2011-2015 (SFI-11/RFP.1/NES/3051).

[1] H. Atmanspacher, in *The Stanford Encyclopedia of Philosophy*, edited by E. N. Zalta (Metaphysics Research Lab, Stanford University, 2015) summer 2015 ed.

[2] D. P. DiVincenzo, Fortschritte der Physik **48**, 771 (2000).

[3] R. Penrose, *The Emperor's New Mind* (Oxford University Press, 1989).

[4] S. Hameroff and R. Penrose, Mathematics and Computers in Simulation **40**, 453 (1996).

[5] S. Hagan, S. R. Hameroff, and J. A. Tuszyński, Physical Review E **65** (2002), 10.1103/physreve.65.061901.

[6] T. J. A. Craddock, S. R. Hameroff, A. T. Ayoub, M. Klobukowski, and J. A. Tuszynski, Current Topics in Medicinal Chemistry **15**, 523 (2015).

[7] W. S. Warren, Science **281**, 247 (1998).

[8] G. S. Engel, T. R. Calhoun, E. L. Read, T.-K. Ahn, T. Mančal, Y.-C. Cheng, R. E. Blankenship, and G. R. Fleming, Nature **446**, 782 (2007).

[9] E. Collini, C. Y. Wong, K. E. Wilk, P. M. G. Curmi, P. Brumer, and G. D. Scholes, Nature **463**, 644 (2010).

[10] G. D. Scholes, G. R. Fleming, L. X. Chen, A. Aspuru-Guzik, A. Buchleitner, D. F. Coker, G. S. Engel, R. van Grondelle, A. Ishizaki, D. M. Jonas, J. S. Lundeen, J. K. McCusker, S. Mukamel, J. P. Ogilvie, A. Olaya-Castro, M. A. Ratner, F. C. Spano, K. B. Whaley, and X. Zhu, Nature **543**, 647 (2017).

[11] S. Huelga and M. Plenio, Contemporary Physics **54**, 181 (2013).

[12] C. Marletto, D. M. Coles, T. Farrow, and V. Vedral, Journal of Physics Communications **2**, 101001 (2018).

[13] L. Hartmann, W. Dür, and H.-J. Briegel, Physical Review A **74** (2006), 10.1103/physreva.74.052304.

[14] J. Li and G. S. Paraoanu, New Journal of Physics **11**, 113020 (2009).

[15] G. Deville, M. Bernier, and J. M. Delrieux, Physical Review B (1979).

[16] G. Eska, H. G. Willers, B. Amend, and C. Wiedemann, Physica B+ C (1981).

[17] R. Bowtell, R. M. Bowley, and P. Glover, Journal of Magnetic Resonance (1969) **88**, 643 (1990).

[18] W. S. Warren, W. Richter, A. H. Andreotti, and B. T. Farmer, Science **262**, 2005 (1993).

[19] E. D. Minot, P. T. Callaghan, and N. Kaplan, Journal of Magnetic Resonance **140**, 200 (1999).

[20] J. Jeener, The Journal of Chemical Physics **112**, 5091 (2000).

[21] R. R. Rizi, S. Ahn, D. C. Alsop, S. Garrett-Roe, M. Mescher, W. Richter, M. D. Schnall, J. S. Leigh, and W. S. Warren, Magnetic Resonance in Medicine **43**, 627 (2000).

[22] C. Zhong, Z. Shaokuan, and Z. Jianhui, Chemical Physics Letters **347**, 143 (2001).

[23] E. Uzi and N. Gil, Journal of Magnetic Resonance **190**, 149 (2008).

[24] J. Baum, M. Munowitz, A. N. Garroway, and A. Pines, Multiple-quantum dynamics in solid state NMR,J. Chem. Phys. 83, 2015 (1985) (1985).

[25] R. Nunes, P. Jezzard, and S. Clare, J Magn Reson **177**, 102 (2005).

[26] D. López-Pérez, *Non-Single Quantum MRI: A Cardiac Modulated Rhythm in the Brain Tissue*, Ph.D. thesis, Medicine, Trinity College Dublin (2016).

[27] J. Słomka and J. Dunkel, Proceedings of the National Academy of Sciences **114**, 2119 (2017).

[28] A. J. Leggett, Journal of Physics C: Solid State Physics **6**, 3187 (1973).

[29] S. I. Doronin, Physical Review A **68** (2003), 10.1103/physreva.68.052306.

[30] B. O. Blair P. Grubb MD, *Syncope: Mechanisms and Management*, 2nd ed. (Wiley-Blackwell, 2005).

[31] W. S. Warren, S. Ahn, M. Mescher, M. Garwood, K. Ugurbil, W. Richter, R. R. Rizi, J. Hopkins, and J. S. Leigh, Science **281**, 247 (1998).

[32] E. F. Gomes, A. M. Jorge, and P. J. Azevedo, in *Proceedings of the International C* Conference on Computer Science and Software Engineering* (ACM, 2013) pp. 23–30.